JOURNAL OF GEOPHYSICAL RESEARCH, VOL. 113, D05212, doi:10.1029/2007JD009052, 2008

Coarse mode optical information retrievable using ultraviolet to short-wave infrared Sun photometry: Application to United Arab Emirates Unified Aerosol Experiment data

N. T. O'Neill,[1] T. F. Eck,[2,3] J. S. Reid,[4] A. Smirnov,[2,3] and O. Pancrati[1]

Received 8 June 2007; revised 13 September 2007; accepted 4 December 2007; published 13 March 2008.

[1] The United Arab Emirates Unified Aerosol experiment provided a unique opportunity for testing aerosol retrieval algorithms in conditions where the optical influence of coarse mode particles was significant. Comparisons between Aerosol Robotic Network (AERONET) Sun photometry retrievals of a previously reported spectral deconvolution algorithm (SDA) and surface-based microphysical and optical measurements showed levels of correlation suggestive of moderate vertical homogeneity for (extensive) measures of fine and coarse mode aerosol particles and stronger vertical homogeneity for indicators of (intensive) aerosol type. An extension of the SDA into the short-wave infrared (SDA+) was developed in order to exploit the enhanced coarse mode information available in new AERONET instruments which include a 1.64 μm channel. Comparisons between values of coarse mode Angstrom exponent (α_c (1.64 μm)) retrieved from SDA+ and effective (coarse mode) radius derived from AERONET inversions showed moderate but significant correlations. Correlations between coarse mode effective radius derived from α_c (1.64 μm) and surface-based volume mean diameter estimates underscored the physical significance of the spectral retrievals and suggested moderate vertical homogeneity in terms of coarse mode particle size.

Citation: O'Neill, N. T., T. F. Eck, J. S. Reid, A. Smirnov, and O. Pancrati (2008), Coarse mode optical information retrievable using ultraviolet to short-wave infrared Sun photometry: Application to United Arab Emirates Unified Aerosol Experiment data, *J. Geophys. Res.*, *113*, D05212, doi:10.1029/2007JD009052.

1. Introduction

[2] The United Arab Emirates Unified Aerosol Experiment (UAE^2) (J. S. Reid et al., A foreword to the United Arab Emirates Unified Aerosol experiment: UAE^2, submitted to *Journal of Geophysical Research*, 2007a) provided a unique opportunity for testing aerosol retrieval algorithms in heterogeneous conditions where the optical influence of coarse mode particles was often significant or dominant. In addition, the array of microphysical and optical measurements acquired during this brief 2 month period (August and September of 2004) yielded an ensemble of independent measurements whose interdependency could be analyzed in order to better understand the dynamics of any single set of optical measurements.

[3] The retrieval of aerosol information from spectral Sun photometry has largely been limited to the spectral region between the ultraviolet (UV) and near-infrared (NIR) wavelengths. Measurements of aerosol optical depth (AOD) in the short-wave infrared (SWIR) spectral region offer increased spectral sensitivity to supermicron (coarse mode) particles at a temporal acquisition rate which is significantly higher and less constrained by cloud contamination than combined retrievals of Sun photometry and sky radiometry (such as the Aerosol Robotic Network (AERONET) retrieval algorithm of *Dubovik et al.* [2002] and *Dubovik and King* [2000]). The recent addition of a 1.64 μm (SWIR) channel to the UV-NIR set of channels employed in the AERONET network has significantly enhanced the spectral information content of data acquired by the instruments in this network (the CIMEL Sun photometer/sky radiometer produced by CIMEL Électronique).

[4] We begin this communication by comparing fine and coarse mode optical depth parameters retrieved using a previously reported UV to NIR spectral deconvolution algorithm (SDA) and fine and coarse mode surface measurements. We then introduce a UV to SWIR extension of the SDA (which we will call SDA+) for the purpose of extracting coarse mode information from SWIR-enhanced AERONET instruments. We then seek to evaluate the physical coherency of the SDA+ technique by comparisons with AERONET

[1] CARTEL, Université de Sherbrooke, Sherbrooke, Quebec, Canada.
[2] NASA Goddard Space Flight Center, Greenbelt, Maryland, USA.
[3] Also at Goddard Earth Sciences and Technology Center, University of Maryland Baltimore County, Baltimore, Maryland, USA.
[4] Naval Research Laboratory, Monterey, California, USA.

0148-0227/08/2007JD009052$09.00

version 2 (AERONET V2) retrieval results and with surface microphysical measurements.

2. Preliminary UV to SWIR Spectral Retrieval Algorithm

[5] The starting point for the SDA+ approach was to require that it be tied to the SDA already developed [*O'Neill et al.*, 2003] for the UV to NIR spectral region. Rather than produce a microphysical-based algorithm, we continued the philosophy of the SDA wherein the retrieval of optical parameters from optical data remains in the optical domain (and depends fundamentally on the measured spectral input parameters of total AOD (τ_a), Angstrom exponent (α), and Angstrom derivative (α')). The means of doing this, aside from employing (visible wavelength) SDA retrieval values as pivot points, is to exploit known asymptotic limits in fine mode Mie spectra and to have the deconvolved fine mode spectra tend toward these limits. The sensitivity of the derived coarse mode parameters to this approach is not high since the fine mode optical depth is almost invariably small in the SWIR region (this is somewhat analogous to the fact that the extraction of fine mode information in the UV-NIR spectral region is not very sensitive to the near-constant spectral behavior of the coarse mode).

[6] The different steps and assumptions involved in the algorithm are defined in Appendix A. The use of a third-order (log τ_a versus log λ) polynomial (spanning the UV to SWIR spectral region) for the total AOD and a fifth-order polynomial (spanning the UV to IR spectral region) for the fine mode optical depth is largely based on polynomial fits applied to Mie simulations [*O'Neill et al.*, 2001]. The approximate empirical relations defining the peak of the fine mode Angstrom exponent ($\lambda_{f,p}$, $\alpha_{f,p}$) were derived from Mie computations over a variety of aerosol types [cf., e.g., *O'Neill et al.*, 2005]. This peak results from the inflection point generated by the increasing predominance of the λ^{-1} absorption trend [*Wickramasinghe*, 1973] over the λ^{-4} scattering trend as the particle size decreases (wavelength increases) in the approach to the small-particle Rayleigh regime. A second asymptotic point is given by the fine mode Angstrom exponent approaching its Rayleigh absorption limit of unity at very small particle size (very large wavelength). The reader will bear in mind that our objectives for the UV-SWIR SDA are to extract coarse mode optical information at a SWIR wavelength where the difference between the total optical parameters and the coarse mode optical parameters is relatively weak (at least for the zeroth-order optical depth and first-order Angstrom exponent).

[7] What degree of coarse mode information actually results from the addition of a SWIR band? One can estimate first-order sensitivity limits in terms of classical Sun photometry: a constraint that can be defined as the condition for which the Angstrom exponent increases with decreasing particle size. The effective Van de Hulst phase shift parameter for a single particle size mode [*O'Neill et al.*, 2005]

$$\rho_{\text{eff}} = 2|m_a - 1|(2\pi r_{\text{eff}}/\lambda) \quad (1)$$

permits one to approximately universalize this condition as being between the peak of the Angstrom exponent at $\rho_{\text{eff}} \sim 0.5$ and the peak of the extinction curve (the anomalous diffraction peak (ADP)) at $\rho_{\text{eff}} \sim 5$. Thus, given $r_{\text{eff}} \sim \rho_{\text{eff}}\lambda/(2\pi)$ (setting $2|m_a - 1| \sim 1$), one can plot the upper and lower r_{eff} limits as a function of the nominal AERONET wavelengths (Figure 1). It can be observed that the 1.64 μm channel begins to straddle the coarse mode-sized region at its lower end and accordingly that this channel is expected to be sensitive to small coarse mode particles such as dust (the volume mean radii of dust being $\sim$1 or 2 μm).

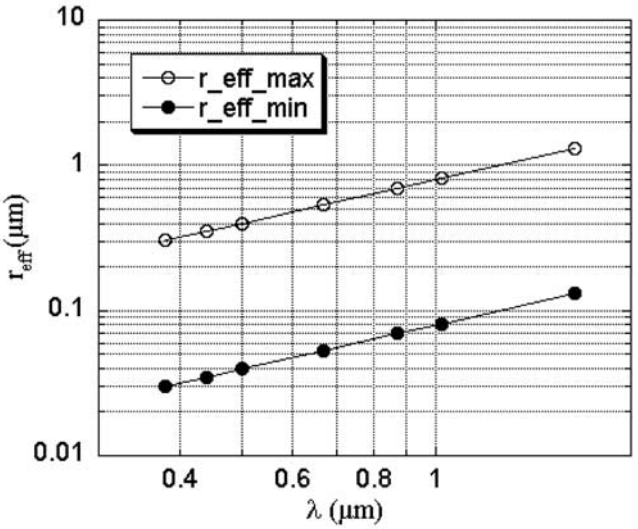

Figure 1. Approximate range of effective radius sensitivity as defined for classical Sun photometry (the condition for which the Angstrom exponent increases with decreasing unimodal particle size). The solid circles correspond to the nominal AERONET wavelengths (the last channel being the 1.64 μm channel).

[8] The graphs on the left sides of Figures 2a and 3a show Mie simulations of $\tau_a(\lambda)$, $\alpha(\lambda)$, $\alpha'(\lambda)$, and $\eta(\lambda)$ spectra for small- and intermediate-sized coarse mode particles, respectively. Various salient spectral features can be noted in each of the two graphs: the dominance of τ_c in the SWIR and the presence of a wavelength peak (around 0.95 μm and greater than 2.0 μm, respectively) corresponding to the traverse of the ADP as particles become optically smaller with increasing wavelength (see *O'Neill et al.* [2005] for other examples), the peak of the fine mode Angstrom exponent due to the scattering/absorption inflection for optically small particles (slightly beyond 2.0 μm), and the novel plotting of fine mode fraction spectra ($\eta(\lambda)$) in the final graph. The peak in τ_c can be computed by employing equation (1) with known input values of $r_{\text{eff},c}$. This yields $\lambda \sim 1.2$ and 2.4 μm for the two cases shown in Figures 2a and 3a (using $r_{\text{eff},c}$ values of 0.95 and 1.90 μm, respectively). Below these wavelengths one enters the (optically) large-particle regime where spectra tend to be relatively flat (the variation of the coarse mode Angstrom exponent is small). The decrease in optical depth with increasing wavelength (beyond the ADP) for these small coarse mode particle cases (readily observable in Figure 2a and just outside the graphing range in Figure 3a) yields small positive values of coarse mode Angstrom exponent at SWIR wavelengths.

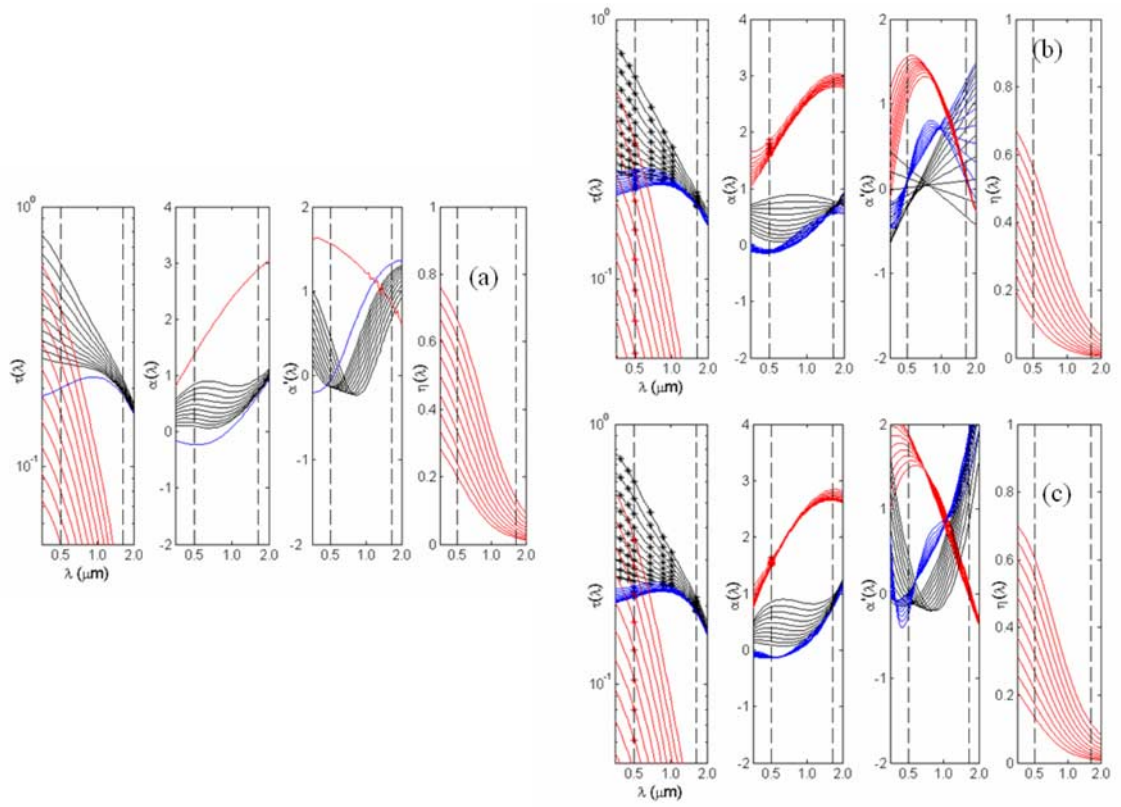

Figure 2. Visible and short-wave infrared (VIS-SWIR) SDA retrievals for Mie simulations applied to lognormal size distributions of fine and coarse mode particles. (a) The $\tau(\lambda)$, $\alpha(\lambda)$, $\alpha'(\lambda)$, and $\eta(\lambda)$ spectra for fixed coarse mode spectra (representative of small coarse mode particles characterized by an $r_{\text{eff},c}$ of 0.95 μm) and a variety of (fixed-size) fine mode spectra whose particle abundance increases in a logarithmic fashion. The black curves represent the total AOD spectra, while the red and blue curves represent fine and coarse spectra, respectively. (b and c) Retrievals obtained for a third- and fourth-order polynomial applied to AERONET-simulated measurements (black asterisks) extracted from the spectra of Figure 2a. Note that the λ and τ axes are logarithmic, while the α, α', and η axes are linear. The vertical dashed lines indicate the spectral position of the 0.5 and 1.64 μm wavelengths.

[9] SDA+ retrievals of fine and coarse mode spectra for the Mie simulations of Figures 2a and 3a are shown in the plots on the left side of the figure (bundles of red and blue curves). Figures 2b and 3b and 2c and 3c correspond to log $\tau(\lambda)$ versus log λ fits to simulated AERONET data (the black asterisks) of third and fourth order, respectively. The increased accuracy of the simulated retrievals in the latter case is often offset by the greater dependence on instrumental and environmental AOD errors which afflict real data; for the retrievals performed in this paper, we elected to err on the conservative side by employing a third-order fit to the total AOD spectra.

3. Sites and Data Employed

[10] AERONET data acquisition protocols, processing algorithms, and instrument placement, within a UAE^2 context, are briefly reviewed by *Eck et al.* [2008]. In order to analyze the results of the UV to SWIR retrieval algorithm, we required SWIR-enhanced AERONET instruments. To evaluate the retrieval of the size-dependent α_c (1.64 μm) parameter, we required that AODs be matched in time to AERONET almucantar retrievals (the frequency of such events being considerably less than the frequency of pure extinction measurements). The nominal input wavelengths for the AERONET instruments whose data were employed for the SDA+ retrievals were 0.38, 0.44, 0.50, 0.675, 0.87, 1.02, and 1.64 μm. The 0.34 μm data were excluded from the analysis because of larger AOD uncertainty at this wavelength [*Eck et al.*, 1999].

[11] Calibration (V_0) results for the new 1.64 μm channel have been typically very stable for both the reference CIMELS calibrated at the Mauna Loa Observatory (MLO) in Hawaii and for field instruments (with performances similar to known stable channels such as the 870 nm channel). The filters themselves have exhibited very stable transmittance over the timescales of 1–3 years (essentially the period over which the new SWIR instruments have been available).

[12] Additionally, there is no detectable temperature sensitivity of the SWIR (indium gallium arsenide) detector at this wavelength. We have seen no variation of τ_c (1.64 μm) at Mauna Loa Observatory (whose values are typically $\ll 0.01$) over the diurnal cycle even though temperature varies by 15°–20°C over the measurement period. Processing includes the subtraction of a small, dynamically measured H_2O optical depth (derived from the 940 nm water vapor channel) and small constant values of CO_2 and methane

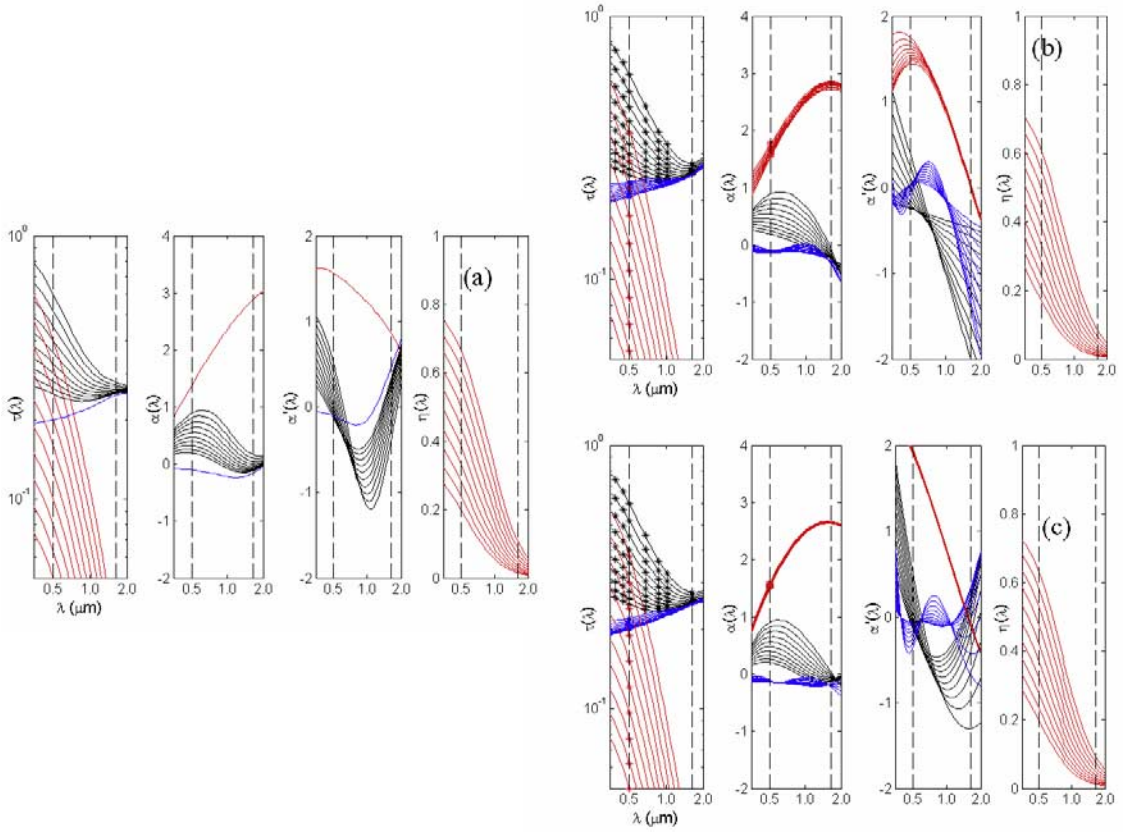

Figure 3. Same as Figure 2 except that the coarse mode spectra represent larger particles characterized by an $r_{\mathrm{eff},c}$ of 1.90 μm.

optical depth. Given all these considerations, we estimate the AOD error to be less than or of the order of 0.005 for master (MLO-calibrated) instruments and $\leq$ 0.01 for field instruments). The undesirable effects of small τ_c (1.64 μm) (especially on a second-order quantity such as α_c (1.64 μm)) were incorporated in the analysis in section 4 by testing results with and without a small-AOD filter.

[13] During UAE^2 there were two SWIR-enhanced instruments located at Dalma and Dhadnah, a SWIR instrument at the NASA Surface-sensing Measurements for Atmospheric Radiative Transfer (SMART) site, and a fourth SWIR instrument at the Mobile Atmosphere Aerosol and Radiation Characterization Observatory (MAARCO) site. We employed only the last three instruments in our analysis inasmuch as the Dalma instrument was known to have larger calibration uncertainties. Since an important part of this paper was simply to evaluate the physical coherency of the SDA+ retrievals, we also employed United Arab Emirates (UAE) data outside the UAE^2 period (Dhabi data from January to July 2004 and Hamim data from July to December 2005). The UAE^2 MAARCO (UV to SWIR) spectra were actually generated from the data of more than one colocated instrument (because of instrument problems in some channels); while 1.64 μm data were available for this "combined" instrument, there were no AERONET almucantar retrievals available at the times when 1.64 μm channel data were acquired (or more precisely, the average interval between the acquisition of almucantar scans and extinction spectra which included 1.64 μm data was considered to be too long). The AERONET almucantar retrievals analyzed in this paper are version 2 retrievals [*Dubovik et al.*, 2006] made without employing AOD and sky radiance measurements at 1.64 μm.

[14] Unless otherwise stated, the data used for the α_c (1.64 μm) part of the analysis corresponded to AOD measurements matched to almucantar times. In addition to ensuring that AERONET retrieval parameters were available for comparison, this provided an additional level of quality-assured data inasmuch as low Sun elevations tend to provide more accurate optical depth data (almucantar retrievals were only performed for solar zenith angles between 50° and 77°) and almucantar cloud screening is more restrictive than solar extinction cloud screening. Since no 1.64 μm optical depths, time matched to almucantar data, were actually available for the MAARCO site, unmatched AOD spectra were used for MAARCO but were restricted to the same zenith angle range as the AERONET retrievals.

[15] Comparisons were made with surface size distribution (aerodynamic particle sizer (APS)) and (TSI 3-λ) nephelometer measurements acquired at the MAARCO site. Details on the APS data and nephelometer data are described by J. S. Reid et al. (Dynamics of southwest Asian dust particle size characteristics with implications for global dust research, submitted to *Journal of Geophysical Research*, 2007b, and Investigation of the mass scattering and extinction efficiency of a heterogeneous mix of pollution and dust particles, submitted to *Journal of Geophysical Research*, 2007c, respectively). The latter measurements were processed using the SDA algorithm (with a first-order

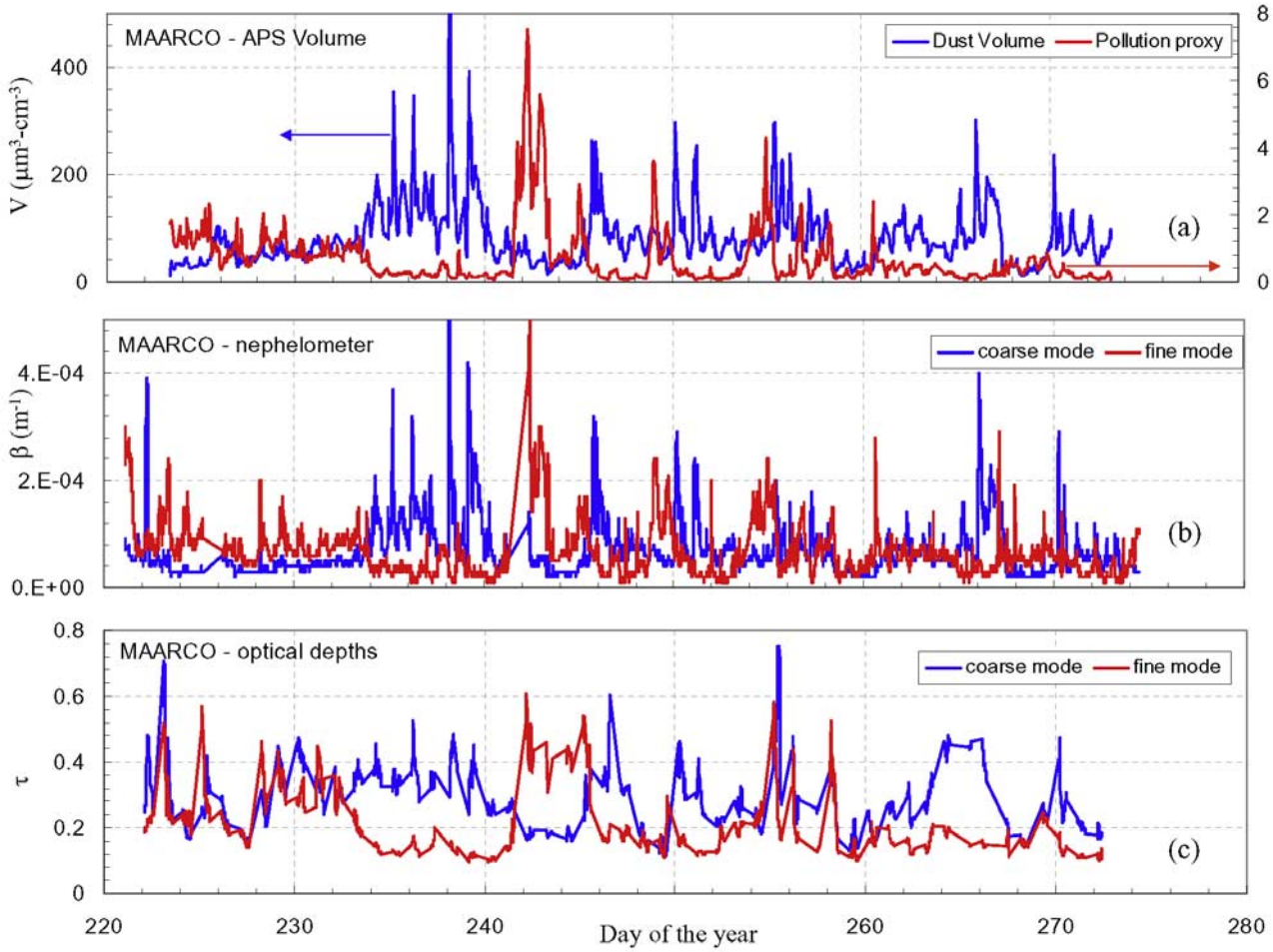

Figure 4. Measured or retrieved parameters at MAARCO: (a) APS measurements of a pollution proxy (fine mode volume for a channel of midbin diameter 0.52 μm) and coarse mode volume (volume integration from 0.8 to 10 μm diameter), (b) SDA retrievals of fine and coarse mode scattering coefficients (β_f and β_c) from three-channel nephelometer data, and (c) SDA retrievals of fine and coarse mode optical depths from CIMEL data. The red and blue curves refer to fine and coarse mode, respectively.

spectral polynomial) applied to the extinction measurements acquired at 0.45, 0.55, and 0.70 μm.

4. Data Analysis

[16] The temporal plots of Figure 4 show the coherency between the fine and coarse mode optical depths at the reference wavelength ($\lambda_r = 0.5$ μm) and the surface measurements at the MAARCO site. The MAARCO site Sun photometer employed for the surface comparisons of Figure 4 was actually an earlier instrument without a 1.64 μm channel (which was not a constraint for the analysis of Figure 4, where the goal was to study SDA-retrieved parameters). Figures 5a–5d show the correlation scattergrams between the optical depth data and the surface measurements (the surface measurements were resampled to the optical depth times). The moderate correlation suggests a degree of vertical mixing for both fine and coarse mode particles (more so for fine mode particles). The similarity of the scattergram patterns for the optical depth versus APS and nephelometer data underscores the strong correlation between the APS and nephelometer measurements (R^2 = 0.86 and 0.80 for the fine and coarse modes, respectively). It is noted that correlation coefficients for the fine mode scattergrams do not change substantially if the outlier points due to the 30 August (day 242) pollution event are removed.

[17] When comparing MAARCO optical depth data to surface nephelometer measurements, Reid et al. (submitted manuscript, 2007c) reported a superior correlation for the Angstrom parameters as compared with the extensive optical parameters (optical depth and scattering coefficient). The superior correlation of the coarse mode fraction ($\eta_c = 1 - \eta$) seen in Figure 5e (as compared with Figures 5c and 5d) underscores this observation; the fine mode fraction (and thus the coarse mode fraction) are linearly related to the Angstrom exponent given that the fine mode particle type varies weakly. One can see this explicitly from the relationships given by *O'Neill et al.* [2003]:

$$\eta_c = 1 - \eta = \frac{\alpha_f - \alpha}{\alpha_f - \alpha_c}, \tag{2}$$

where the fine mode Angstrom exponent (α_f) varies only weakly relative to α. As pointed out by Reid et al.

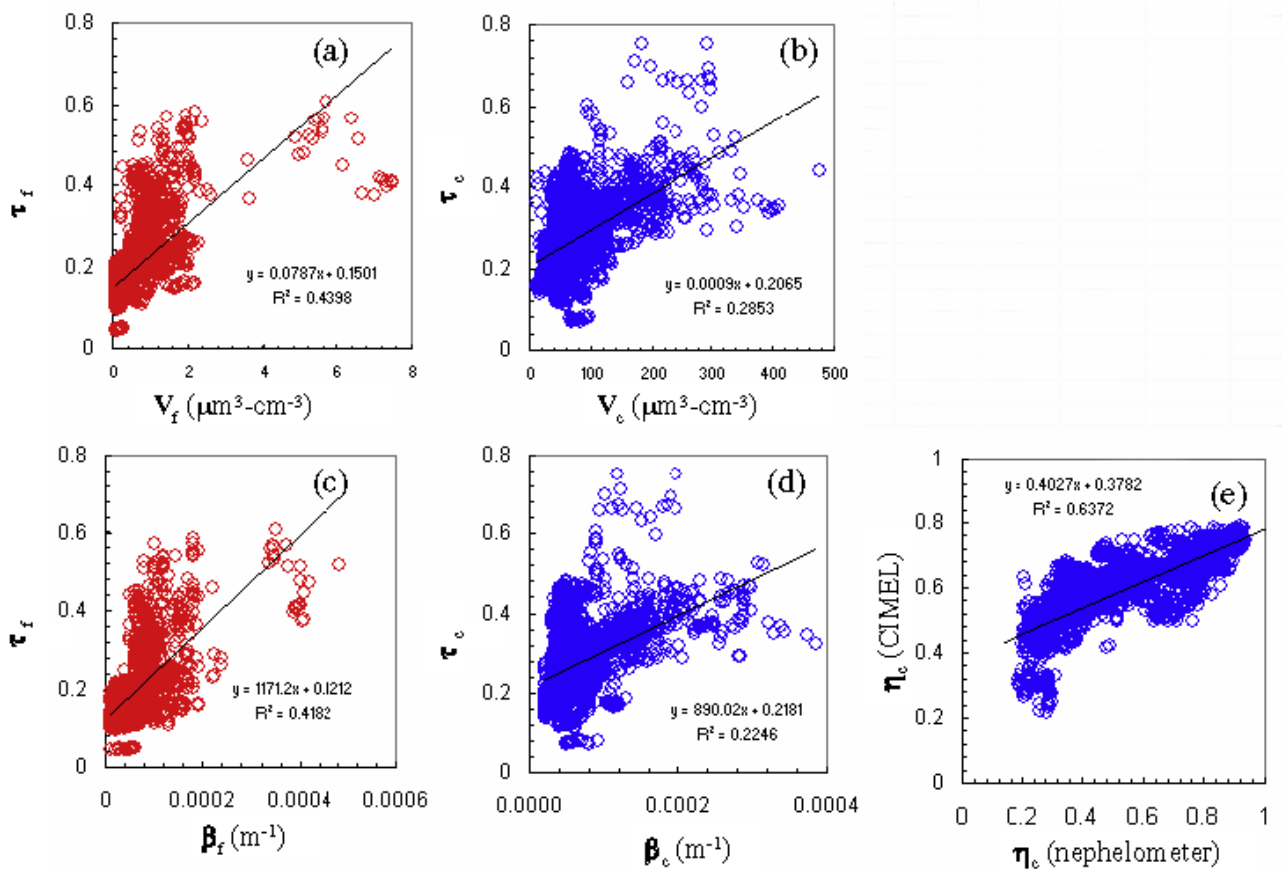

Figure 5. Correlation scattergrams between the fine and coarse mode parameters of Figure 4. (a and b) Fine and coarse mode optical depths versus their APS volume analogues. (c and d) Fine and coarse mode optical depths versus their nephelometer scattering-coefficient analogues. Temporal synchronization was achieved by resampling the APS and nephelometer data to the times of the optical depth data. Same color key as employed in Figure 4. (e) Correlation graph between the coarse mode fraction ($\eta_c = 1 - \eta$) from the optical depth data versus the coarse mode fraction from the nephelometer data.

(submitted manuscript, 2007c), this suggests a higher degree of vertical homogeneity for aerosol type; in terms of Figure 5 this means that the coarse mode fraction is an intensive parameter which is only dependent on the relative quantities of fine and coarse mode particles.

[18] Figure 6 shows SDA+ results for a sampling of spectra from four sites in the UAE region. The four graphs, from Figure 6a to Figure 6d, show the general features of the Mie simulations in Figures 2 and 3 with increasing $\tau_c(\lambda)$ maxima between 1 and 2 μm wavelength corresponding to decreasing values of α_c (1.64 μm). The spectral curves depart significantly from the Mie spectra in the $\alpha'(\lambda)$ curves because of the sensitivity of this spectral parameter to small changes in optical depths and because of the choice of a third-order polynomial for the retrieved total optical depths (which, for example, must necessarily result in a linear, and probably artificial, dependence for the computed values of $\alpha'(\lambda)$). As indicated above, this third-order choice is a tradeoff between higher-order polynomials (greater degrees of freedom) and the sensitivity to noisy (anomalous high-frequency) effects in the measured AOD spectra.

[19] Figure 7 illustrates some interesting scattergrams for optical parameters derived from AOD spectra acquired at the SMART site. The y axis is the value of τ_c (1.64 μm) derived from SDA+; the red and blue symbols show the dispersion relative to SDA-derived values of τ_f (0.5 μm) and τ_c (0.5 μm), respectively, while the purple values show the dispersion relative to the classical Angstrom parameter (β). The latter parameter is nominally an estimate of the total AOD at 1 μm and thus has long been claimed to be an indicator of coarse mode optical depth (it is very strongly associated with the measured AOD (1.02 μm); for the data of Figure 7, AOD (1.02 μm) = 0.9891β + 0.0063 with an R^2 = 0.9974). The lack of general correlation with τ_f (0.5 μm) and the strong correlation with τ_c (0.5 μm) underscore the independence of these two parameters and an optophysical coherency in the SDA+ approach. The large τ_f (0.5 μm) outliers lying almost parallel to the x axis represent the pollution events between 30 August and 3 September (day 242 to day 246) and between 10 September and 14 September (day 254 to day 258) (removal of these pollution days results in a correlation coefficient increase to R^2 = 0.17). The relatively strong correlation of τ_c (1.64 μm) with β is consistent with the arguments for β being a measure of coarse mode optical depth, while the subunity slope of the regression line is a consequence of the AOD at 1 μm being approximately a maximum (because λ = 1 μm is near the ADP).

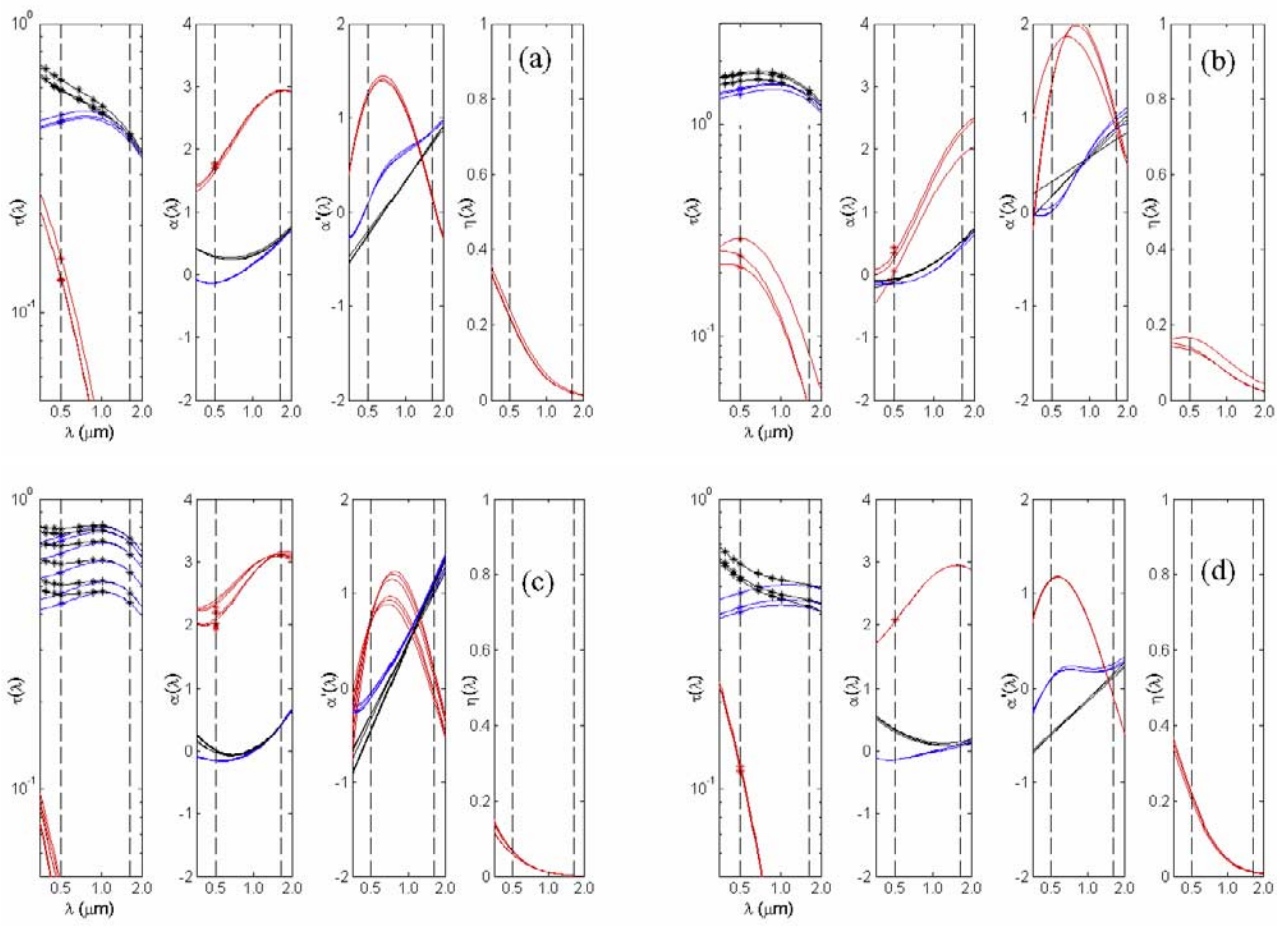

Figure 6. Illustration of retrieved VIS to SWIR spectra (same color key and interpretation as Figures 2 and 3). The four graphs show progressively decreasing values of α_c (1.64 μm): (a) SMART site, 25 August 2004 (UAE^2 period), (b) Blida site, 21 February 2004 (pre-UAE^2 period), (c) Dhabi site, 14 December 2003 (pre-UAE^2 period), and (d) SMART site, 11 August 2004 (UAE^2 period).

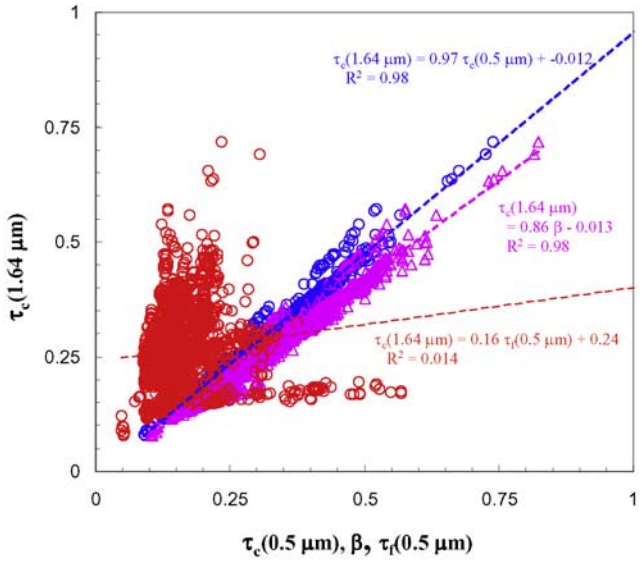

Figure 7. Retrieved coarse mode optical depth at 1.64 μm for the SMART data as a function of the coarse mode optical depth retrieved at the reference wavelength of $\lambda_r = 0.5$ μm (blue), the Angstrom Beta exponent (purple), and the fine mode optical depth at 0.5 μm (red).

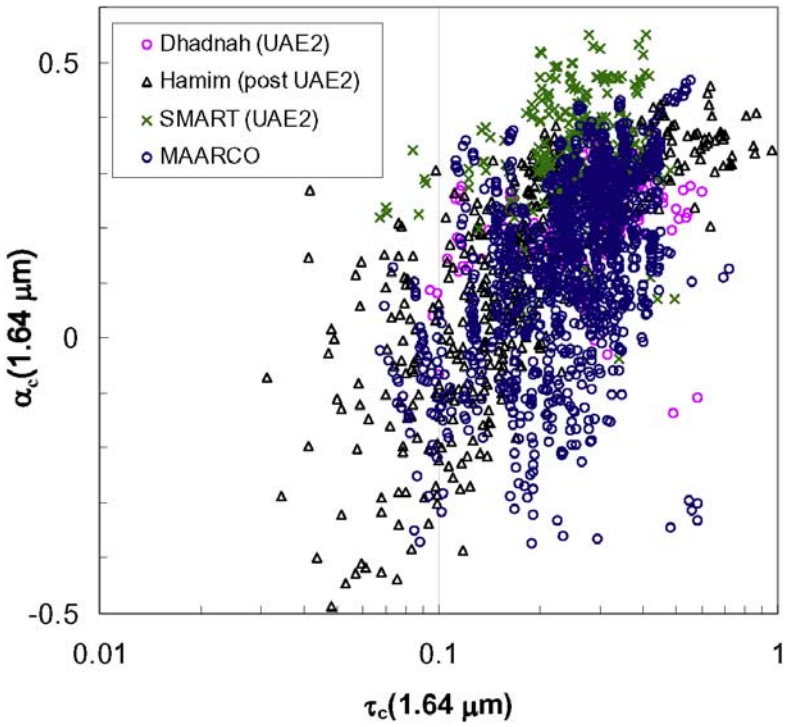

Figure 8. Retrieved value of α_c (1.64 μm) versus τ_c (1.64 μm) for the SMART, Dhadnah MAARCO, and Hamim sites of Table 1 (no-filtering case).

[20] A scattergram of α_c (1.64 μm) versus τ_c (1.64 μm) is shown in Figure 8 for all retrieval sites with the exception of the pre-UAE^2 site of Dhabi. Regression results for all retrieval sites (including the effects of filtering for small τ_c (1.64 μm) less than 0.2) are shown in Table 1. The motivation for this type of plot was to mimic the classic α versus τ_a type of graphic where the dynamics between size and aerosol burden (intensive and extensive optical parameters) can be succinctly illustrated on a 2-D graph. The large variation for small τ_c (1.64 μm) is likely influenced by the extreme sensitivity of Angstrom-type slopes to fixed AOD uncertainties in the presence of small AODs [see, e.g., *O'Neill et al.*, 2001]. While the unfiltered scattergram of Figure 8 appears to show a general positive correlation with τ_c (1.64 μm) (a decrease in coarse mode particle size with increasing coarse mode abundance), the versions filtered for small τ_c (1.64 μm) show little to marginal positive correlation (see Table 1 where the MAARCO data yielded the only marginal correlation). The Dhabi data set actually showed a systematic decrease in α_c (1.64 μm) with τ_c (1.64 μm) which was independent of filtering conditions. However, the Dhabi values of Angstrom exponent, with values ranging between 0.3 and 2.0, were felt to be systematically and significantly overestimated and thus were not included in Figure 8 (compare this with the analysis of Table 2).

[21] Figure 9 is a sample scattergram between SDA+ values of α_c (1.64 μm) and $r_{\mathrm{eff},c}$ values derived from AERONET V2 almucantar inversions (for the Dhadnah UAE^2 data). The green curve (whose regression parameters are shown in bold at the bottom of Table 2) is a regression line through a series of Mie computations using 19 different types of coarse mode lognormal size distributions which were based on a variety of AERONET coarse mode almucantar retrievals. It is noted that there are more universal empirical expressions for the effective radius of a unimodal size distribution which involve α' as well as α [*O'Neill et al.*, 2005]. However, such expressions would do no better than the Mie regression line of Figure 9 in the limited size range being analyzed here (and maybe worse given the apparently unstable nature of α'). For this reason and because we wished to maintain a simple monotonic link between $r_{\mathrm{eff},c}$ and α_c (1.64 μm), we chose to employ the simpler Mie regression between these two parameters. These computations were checked for the effects of nonsphericity using the computations of *Mischenko et al.* [1997] as a guide; for the

Table 1. Correlation Between α_c (1.64 μm) and τ_c (1.64 μm)[a]

	No Filtering				$\tau_c > 0.1$				$\tau_c > 0.2$			
	m	*b*	R^2	*N*	m	*b*	R^2	*N*	m	*b*	R^2	*N*
Dhadnah (UAE^2)	0.223	0.15	0.07	178	0.166	0.169	0.04	174	0.114	0.188	0.01	144
SMART (UAE^2)	0.222	0.287	0.03	245	0.177	0.301	0.02	238	−0.08	0.385	0	194
MAARCO (UAE^2)	0.71	−0.04	0.19	1270	0.632	−0.02	0.14	1223	0.453	0.046	0.06	936
Dhabi (2004, pre-UAE^2)	−1.04	1.064	0.33	494	−0.63	0.919	0.26	373	−0.43	0.83	0.21	180
Hamim (2005, post-UAE^2)	0.829	−0.07	0.39	463	0.627	0.01	0.38	373	0.244	0.201	0.2	180

[a]The parameters, *m*, *b*, and R^2 are the slope, intercept, and correlation coefficient, respectively, of α_c (1.64 μm) versus τ_c (1.64 μm).

Table 2. Correlation Between α_c (1.64 μm) and $r_{\text{eff},c}$ From the AERONET Version 2 Retrieval[a]

	No Filtering				$\tau_c > 0.2$				$\tau_c > 0.2$, $\Delta\alpha < 0.075$			
	m	*b*	R^2	*N*	m	*b*	R^2	*N*	m	*b*	R^2	*N*
Dhadnah (UAE^2)	−0.29	0.781	0.28	178	−0.3	0.799	0.2	144	−0.25	0.754	0.46	84
SMART (UAE^2)	−0.38	1.07	0.39	245	−0.4	1.11	0.4	194	−0.37	1.071	0.5	169
Dhabi (2004, pre-UAE^2)	−0.35	1.465	0.07	494	−0.47	1.495	0.43	180	−0.47	1.497	0.42	177
Hamim (2005, post-UAE^2)	−0.48	1.029	0.09	463	−0.47	1.171	0.36	180	−0.35	0.982	0.38	144
Mie	**−0.41**	**0.932**	**0.7**	**19**								

[a]The parameters, *m*, *b*, and R^2 are the slope, intercept, and correlation coefficient, respectively, of α_c (1.64 μm) versus $r_{\text{eff},c}$.

collection of sample distributions, τ_c (1.64 μm) was estimated to change by less than 10% in going from spherical to spheroid computations while α_c (1.64 μm) changed by less than 0.1.

[22] The moderate correlation observed for the four test cases shown in Table 2 was improved by restricting both τ_c (1.64 μm) to larger values and $\Delta\alpha = \alpha$ (1.64 μm) − α_c (1.64 μm) to smaller values. That the improved range of correlations obtained in the latter case was not larger is in no small measure related to the fact that the Mie correlation itself is fairly dispersive ($R^2 = 0.7$). The Dhabi correlation values were about the same order of magnitude, but the amplitude of α_c (1.64 μm) was significantly overestimated (as indicated by the intercept values which were more than 50% greater than the Mie intercepts).

[23] The temporal plots of Figure 10 lend credence to the use of α_c (1.64 μm) as an indicator of coarse mode size. The two graphs show high-frequency and low-frequency comparisons between the VMD derived from the MAARCO surface volume (APS) measurements and 2 × $r_{\text{eff},c}$, where $r_{\text{eff},c}(\alpha_c)$ is obtained from the linear Mie expression given in Table 2. This latter quantity is less an attempt to compare optically derived size estimates with surface VMD values than to demonstrate that there exists a degree of weak but significant positive correlation between these two independent sources of coarse mode size ($R^2 = 0.27$ for the daily average case). That the correlation can be seen at both high and low frequencies (hourly and daily averages for the APS) is not only an indirect validation of the optical technique but also suggests a measure of vertical homogeneity in terms of coarse mode particle size. The latter observation is in keeping with the general observations on regional homogeneity during UAE^2 made by *Eck et al.* [2008] and J. S. Reid et al. (Observations of summertime atmospheric thermodynamic and aerosol profiles of the southern Arabian Gulf, submitted to *Journal of Geophysical Research*, 2007d). Although this observation is analogous to the observation made above concerning the greater vertical homogeneity of η_c(CIMEL) (compared with τ_f and τ_c at 500 nm), that case concerned the relative vertical variation of the optical depths (largely induced by abundance variations) while the discussion here relates to the vertical homogeneity of coarse mode particle size.

5. Summary and Conclusions

[24] A spectral deconvolution algorithm (SDA+) for the extraction of fine and coarse mode optical spectra from the UV to the SWIR spectral region was defined by tying the retrieved spectra to the results of a UV to NIR spectral deconvolution algorithm and to the known asymptotic Rayleigh limits of optically small particles. The retrieved spectra showed a variety of spectral features which were consistent with expectations given the underlying Mie theory (some of these features, notably the fine mode spectral properties, being forced by the assumptions of the SDA+ retrieval). Comparisons between the SDA results and surface-based microphysical measurements showed levels of (temporal) correlation which were suggestive of moderate vertical homogeneity for extensive measures of fine and coarse mode aerosol particles and stronger vertical homogeneity for indicators of (intensive) aerosol type. The retrieved SDA+ spectra were found to yield values of τ_c (1.64 μm) which were strongly correlated with SDA-derived τ_c (0.5 μm) values and largely uncorrelated with τ_f (0.5 μm) values. Plots of α_c (1.64 μm) versus τ_c (1.64 μm) showed little or only marginal correlation, suggesting only a weak dependence between coarse mode particle size and coarse mode particle loading. Comparisons between α_c (1.64 μm) and values of $r_{\text{eff},c}$ derived from version 2 AERONET inversions showed significant correlations which, with proper filtering of small optical depths, were only moderately inferior to the correlation expected from Mie optics. Correlations between $r_{\text{eff},c}$ derived from α_c (1.64 μm) and surface-based VMD estimates from APS

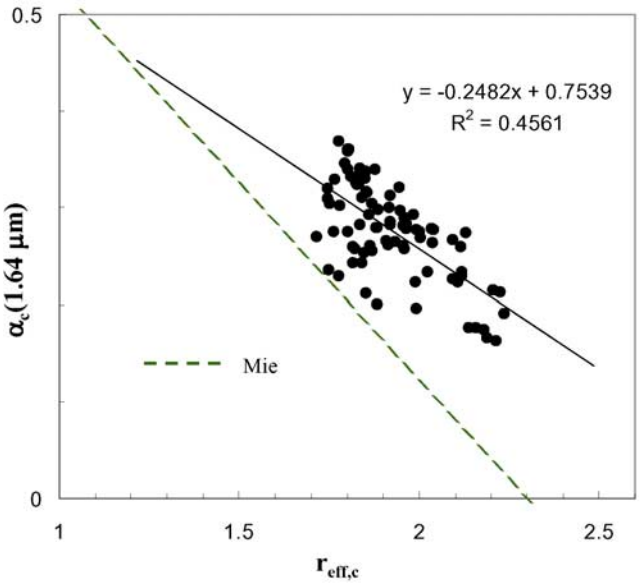

Figure 9. Sample scattergram between α_c (1.64 μm) from the SDA+ algorithm and $r_{\text{eff},c}$ from AERONET version 2 retrievals for the Dhadnah UAE^2 data (filtered case of $\tau_c > 0.2$, $\Delta\alpha = \alpha$ (1.64 μm) − α_c (1.64 μm) < 0.075).

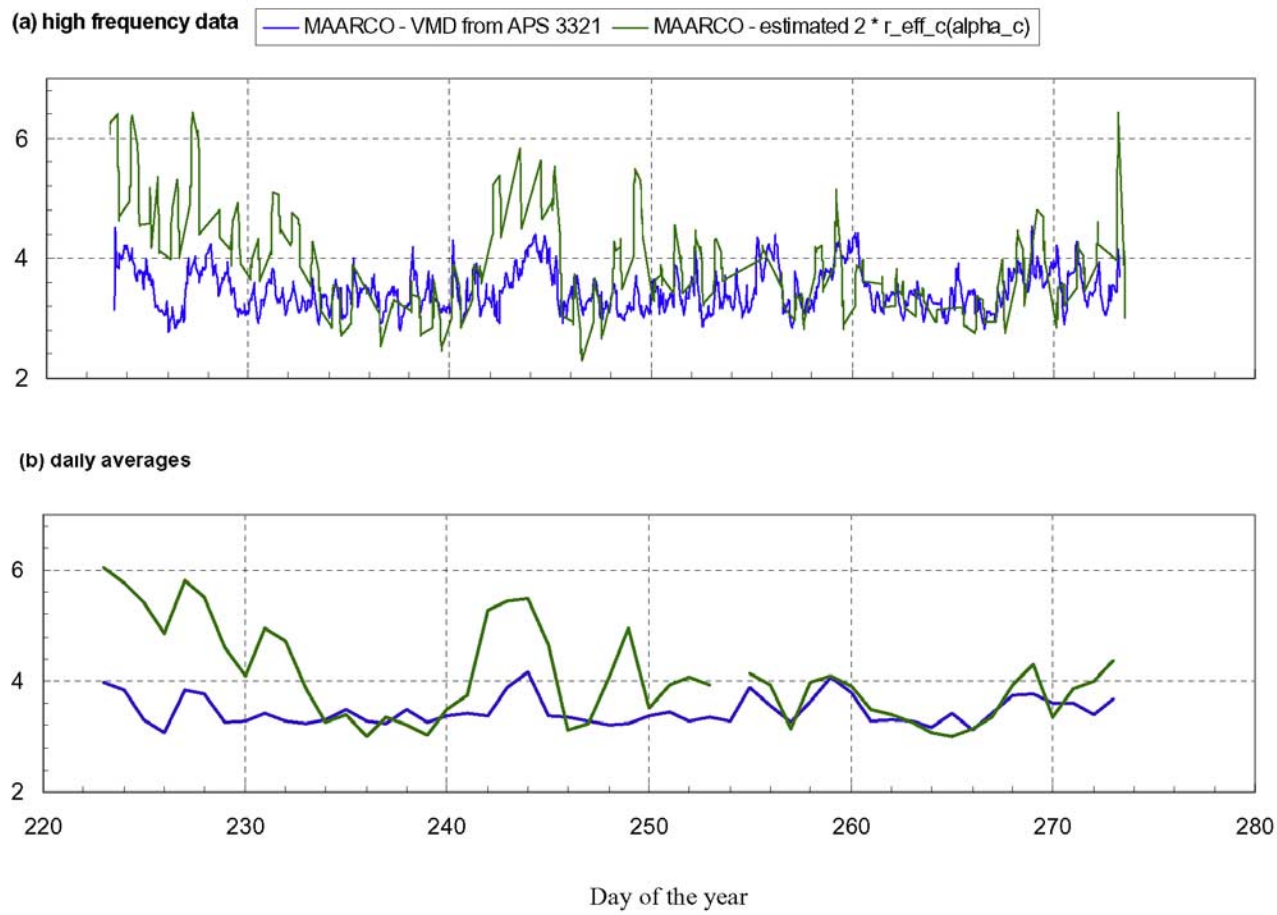

Figure 10. Temporal profiles of VMD derived from the MAARCO APS instrument and $2r_{\mathrm{eff},c}$ values derived from α_c (1.64 μm) using an approximate Mie relationship between $r_{\mathrm{eff},c}$ and α_c (1.64 μm).

data helped to further validate the spectral retrievals and suggested a degree of vertical homogeneity in terms of coarse mode particle size.

Appendix A: SDA+ Algorithmic Steps

[25] 1. Compute $\tau_a(\lambda)$, $\alpha(\lambda)$, and $\alpha'(\lambda)$ from a third-order spectral polynomial applied to the UV, VIS, NIR, and SWIR wavelengths [cf. *O'Neill et al.*, 2001, section 3.3].

[26] 2. Use the SDA algorithm of *O'Neill et al.* [2003] to compute τ_a, τ_f, τ_c, α_f, α_f', and $\eta = \tau_f/\tau_a$ at a reference or pivot wavelength of λ_r (normally 500 nm).

[27] 3. Employ a fifth-order polynomial for $\tau_f(\lambda)$, fourth-order polynomial for $\alpha_f(\lambda)$, and third-order polynomial for $\alpha_f'(\lambda)$ in a set of simultaneous equations to solve for the polynomial coefficients of the fine mode optical depth spectrum. Step 3 has three parts.

[28] First, $\tau_f(\lambda)$, $\alpha_f(\lambda)$, and $\alpha_f'(\lambda)$ go through $\tau_f(\lambda_r)$, $\alpha_f(\lambda_r)$, and $\alpha_f'(\lambda_r)$.

[29] Second, $\alpha_f(\lambda)$ and $\alpha_f'(\lambda)$ go through $\alpha_{f,p} = \alpha_f(\lambda_{f,p})$ (the peak in α_f) and $\alpha_{f,p}' = \alpha_f'(\lambda_{f,p})$, where

$$\lambda_{f,p} = -0.8\alpha_f + 3.0\mu\mathrm{m} \tag{A1}$$

$$\alpha_{f,p} = \alpha_f + 0.91\left(\lambda_{f,p} - \lambda_r\right) - 0.04, \alpha_{f,p}' = 0. \tag{A2}$$

[30] Third, $\alpha_f(\lambda)$ and $\alpha_f'(\lambda)$ go through $\alpha_{f,R} = \alpha_f(\lambda_{f,R})$ and $\alpha_{f,R}' = \alpha_f'(\lambda_{f,R})$, the Rayleigh absorption limit, (min λ for which $2\pi r_{\mathrm{eff}}|\mathrm{m} - 1|/\lambda \leq 0.1$), where

$$\lambda_{f,R} = 12\mu\mathrm{m} \tag{A3}$$

$$\alpha_{f,R} = 1, \alpha_{f,R}' = 0. \tag{A4}$$

[31] 4. Compute coarse mode parameters given the total and fine mode spectra from the previous step and using equations (4) and (5) of *O'Neill et al.* [2001]:

$$\tau_c(\lambda) = \tau_a(\lambda) - \tau_f(\lambda), \quad \eta = \tau_f(\lambda)/\tau_a(\lambda) \tag{A5}$$

$$\alpha_c(\lambda) = \left(\alpha(\lambda) - \eta\alpha_f(\lambda)\right)/(1-\eta) \tag{A6}$$

$$\alpha_c'(\lambda) = \left(\alpha'(\lambda) - \eta\alpha_f'\right)/(1-\eta) + \eta\left(\alpha_f - \alpha_c\right)^2. \tag{A7}$$

Notation

α_f instantaneous slope of $-\ln \tau_f$ versus $\ln \lambda$, dimensionless.

α_c instantaneous slope of $-\ln \tau_c$ versus $\ln \lambda$, dimensionless.

α instantaneous slope of $-\ln \tau_a$ versus $\ln \lambda$, dimensionless.

α'_f instantaneous slope of α_f versus ln λ, dimensionless.
α'_c instantaneous slope of α_c versus ln λ, dimensionless.
α' instantaneous slope of α versus ln λ, dimensionless.
b linear regression intercept, units depend on usage. Employed in Tables 1 and 2.
β Angstrom coefficient, (from $\tau_a = \beta\ \lambda^{-\alpha}$).
β_c coarse mode scattering coefficient derived from nephelometer data [m^{-1}].
β_f fine mode scattering coefficient derived from nephelometer data [m^{-1}].
β_a total scattering coefficient from nephelometer data [m^{-1}].
η fine mode fraction, τ_f/τ_a, dimensionless.
η_c coarse mode fraction, $\tau_c/\tau_a = 1 - \eta$, dimensionless. Defined in equation (2).
λ wavelength [μm].
λ_r reference wavelength for the SDA algorithm, typically chosen as 0.5 μm [μm].
m linear regression slope, dimensionless. Employed in Tables 1 and 2.
m_a complex refractive index, dimensionless.
N number of measurements in a given data set, dimensionless.
R^2 square of the correlation coefficient for a linear regression, dimensionless.
r_{eff} optically effective radius of a unimodal size distribution [μm].
$r_{\text{eff},c}$ effective radius of the coarse mode particle size distribution [μm].
ρ_{eff} effective phase shift parameter of a unimodal size distribution, dimensionless. Defined in equation (1).
τ_c coarse mode optical depth, dimensionless.
τ_f fine mode optical depth, dimensionless.
τ_a total aerosol extinction optical depth (AOD), $\tau_f + \tau_c$, dimensionless.
V_c coarse mode particle volume per unit volume, $\mu m^3\ cm^{-3}$.
V_f proxy for fine mode particle volume per unit volume, $\mu m^3\ cm^{-3}$.

[32] **Acknowledgments.** The authors would like to thank the National Sciences and Engineering Research Council of Canada, the Canadian Foundation for Climate and Atmospheric Sciences, and Le Fonds québécois de la recherche sur la nature et les technologies for their financial support. Valuable in-kind support was obtained from the Meteorological Services of Canada and NASA's AERONET project. The contributions of Ilya Slutsker and David Gilles of the AERONET group are gratefully acknowledged.

References

Dubovik, O., and M. D. King (2000), A flexible inversion algorithm for retrieval of aerosol optical properties from Sun and sky radiance measurements, *J. Geophys. Res.*, *105*, 20,673–20,696.

Dubovik, O., B. N. Holben, T. Lapyonok, A. Sinyuk, M. I. Mishchenko, P. Yang, and I. Slutsker (2002), Non-spherical aerosol retrieval method employing light scattering by spheriods, *Geophys. Res. Lett.*, *29*(10), 1415, doi:10.1029/2001GL014506.

Dubovik, O., et al. (2006), Application of spheroid models to account for aerosol particle nonsphericity in remote sensing of desert dust, *J. Geophys. Res.*, *111*, D11208, doi:10.1029/2005JD006619.

Eck, T. F., B. N. Holben, J. S. Reid, O. Dubovik, A. Smirnov, N. T. O'Neill, I. Slutsker, and S. Kinne (1999), Wavelength dependence of the optical depth of biomass burning, urban, and desert dust aerosols, *J. Geophys. Res.*, *104*, 31,333–31,349.

Eck, T. F., et al. (2008), Spatial and temporal variability of column-integrated aerosol optical properties in the southern Arabian Gulf and United Arab Emirates in summer, *J. Geophys. Res.*, *113*, D01204, doi:10.1029/2007JD008944.

Mishchenko, M. I., L. D. Travis, R. A. Kahn, and R. A. West (1997), Modeling phase functions for dustlike tropospheric aerosols using a shape mixture of randomly oriented polydisperse spheroids, *J. Geophys. Res.*, *102*, 16,831–16,847.

O'Neill, N. T., T. F. Eck, B. N. Holben, A. Smirnov, O. Dubovik, and A. Royer (2001), Bimodal size distribution influences on the variation of Angstrom derivatives in spectral and optical depth space, *J. Geophys. Res.*, *106*, 9787–9806.

O'Neill, N. T., T. F. Eck, A. Smirnov, B. N. Holben, and S. Thulasiraman (2003), Spectral discrimination of coarse and fine mode optical depth, *J. Geophys. Res.*, *108*(D17), 4559, doi:10.1029/2002JD002975.

O'Neill, N. T., S. Thulasiraman, T. F. Eck, and J. S. Reid (2005), Robust optical features of fine mode size distributions: Application to the Québec smoke event of 2002, *J. Geophys. Res.*, *110*, D11207, doi:10.1029/2004JD005157.

Wickramasinghe, N. C. (1973), *Light Scattering Functions for Small Particles, With Applications in Astronomy*, 506 pp., Wiley, New York.

T. F. Eck and A. Smirnov, NASA Goddard Space Flight Center, Greenbelt, MD 20771, USA.

N. T. O'Neill and O. Pancrati, CARTEL, Université de Sherbrooke, Sherbrooke, QC, Canada J1K 2R1. (norm.oneill@usherbrooke.ca)

J. S. Reid, Naval Research Laboratory, 7 Grace Hopper Avenue, Stop 2, Monterey, CA 93943-5502, USA.